Polymer Journal
https://doi.org/10.1038/s41428-026-01156-7

ORIGINAL ARTICLE

Preparation of urea-containing polysilsesquioxane membranes for CO_2 separation designed by model-based research

Yusuke Kanematsu[1] · Katsuhiro Horata[1] · Kazuki Hara[1] · Yohei Adachi[1] · Toshinori Tsuru[2] · Masakoto Kanezashi[2] · Joji Ohshita[1,3]

Received: 19 November 2025 / Revised: 13 January 2026 / Accepted: 19 January 2026

Abstract

Membrane separation has been extensively studied as a cost-effective CO_2 separation method, and polysilsesquioxane (PSQ)-based membranes are expected to be robust membranes with high thermal and mechanical stability and processability. In this study, a prediction model for CO_2 permeance and CO_2/N_2 permselectivity as target variables was generated by applying machine learning to experimental data collected in our previous studies as explanatory variables. On the basis of this model, two new urea-containing PSQ-based membranes were prepared, and their CO_2 separation performance was evaluated. Among them, a membrane synthesized through the 1:1 copolymerization of (3,6-dioxaoctane-1,8-diyl)bis-*N*-[*N*'-(triethoxysilylpropyl)urea] and bis(triethoxysilyl)ethane demonstrated high performance, achieving a CO_2 permeance of 1.3×10^{-6} mol $m^{-2}s^{-1}Pa^{-1}$ (4.0×10^3 GPU) and a CO_2/N_2 permselectivity of 13. A membrane was also prepared using (triethylamine-2,2',2"-triyl)tris-*N*-[*N*'-(triethoxysillylpropyl)urea] as a monomer, which resulted in inferior CO_2 separation performance. However, increasing the calcination temperature significantly increased the CO_2 permeance, whereas the CO_2/N_2 permselectivity slightly decreased, likely because of the thermal degradation of the urea units, resulting in the formation of void spaces.

Introduction

Reducing CO_2 emissions is crucial on a global scale, and membrane separation has been extensively studied as a cost-effective method for CO_2 separation. There are various categories of CO_2 separation membranes, including organic and inorganic membranes [1–5], mixed-matrix membranes (MMMs), and metal–organic framework (MOF) membranes [6, 7]. Several mechanisms have been recognized for CO_2 separation [8–10], such as molecular sieving effects, which allow smaller gas molecules to permeate the membrane more rapidly through a porous structure than larger molecules do. Additionally, the diffusion of gas molecules to the pore surface effectively enhances transport in porous membranes, particularly when the pore surface has an affinity for CO_2 molecules. For nonporous membranes, the dissolution permeation of CO_2 molecules through the membrane facilitates transport, where the CO_2 affinity influences membrane performance through its effect on the CO_2 dissolution capacity. Generally, the diffusivity and solubility of CO_2 molecules are enhanced by membrane CO_2 affinity. Therefore, diffusion- and solubility-based CO_2 transport accelerates with decreasing operation temperature, although reduced molecular mobility suppresses transport to some extent. However, an excessively high affinity may result in the tight capture of CO_2 molecules, which in turn inhibits their transport.

Polysilsesquioxanes (PSQs) have garnered significant attention as durable materials owing to their excellent

Supplementary information The online version contains supplementary material available at https://doi.org/10.1038/s41428-026-01156-7.

✉ Yusuke Kanematsu
ykanem@hiroshima-u.ac.jp

✉ Masakoto Kanezashi
kanezashi@hiroshima-u.ac.jp

✉ Joji Ohshita
jo@hiroshima-u.ac.jp

[1] Smart Innovation Program, Graduate School of Advanced Science and Engineering, Hiroshima University, Higashi-Hiroshima, Japan

[2] Chemical Engineering Program, Graduate School of Advanced Science and Engineering, Hiroshima University, Higashi-Hiroshima, Japan

[3] Division of Materials Model-Based Research, Digital Monozukuri (Manufacturing) Education and Research Center, Hiroshima University, Higashi-Hiroshima, Japan

Published online: 13 March 2026

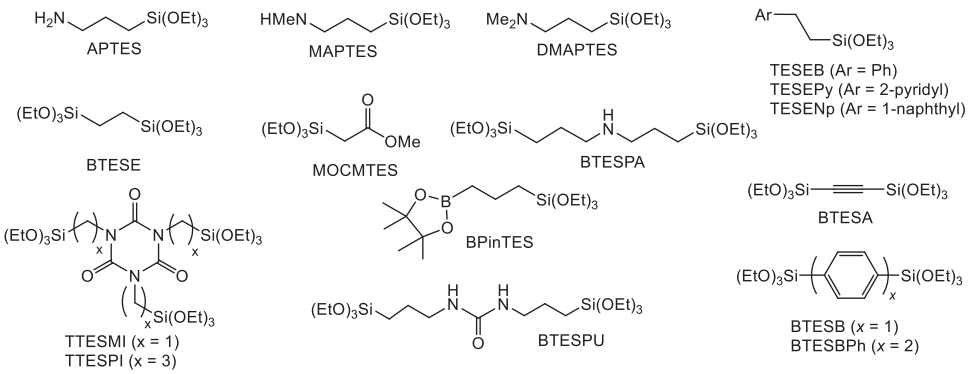

Fig. 1 Examples of precursors of PSQ-based CO_2 separation membranes

thermal and mechanical stabilities and ease of processing. This is attributed to their inorganic siloxane network structure combined with organic groups attached to silicon atoms [11–14]. These materials are readily accessible via the hydrolysis condensation polymerization of trifunctional organosilicon monomers, such as trialkoxysilanes. PSQ-based CO_2 separation membranes have also been studied, and it has been demonstrated that their performance is significantly influenced by PSQ organic groups [15–30]. For example, a membrane prepared from a monomer with a primary amine unit (APTES in Fig. 1) exhibited CO_2 separation properties [17–22] with P_{CO2} (CO_2 permeance) $= 2.6 \times 10^{-8}$ mol m^{-2}s^{-1}Pa^{-1} and CO_2/N_2 (CO_2/N_2 permselectivity) $= 22$, whereas the use of a tertiary amine monomer (DMAPTES) improved the CO_2 permeance to a value of 1.72×10^{-7} mol m^{-2}s^{-1}Pa^{-1}, with CO_2/N_2 permselectivity remaining at a similar level ($CO_2/N_2 = 21$) [17, 18]. Employing secondary amine MAPTES as the monomer resulted in a decrease in both CO_2 permeance and CO_2/N_2 permselectivity ($P_{CO2} = 1.7 \times 10^{-8}$ mol m^{-2}s^{-1}Pa^{-1} and $CO_2/N_2 = 11$). Because DFT calculations indicated that the amine initially interacts with CO_2 as a base to form N--C(O_2) coordination rather than an acid with hydrogen bonding to CO_2 in the manner of NH--O(CO), tertiary amines would possess a higher CO_2 affinity than primary amines would. However, primary and secondary amines can form ionic complexes with CO_2 ($RNHCO_2^-$ RNH_3^+ and $R_2NCO_2^-$ $R_2NH_2^+$), which may hinder CO_2 transport [31]. Steric hindrance arising from the methyl group may also affect the performance; however, the reason for the lower performance of the MAPTES membrane than that of the APTES membrane is still unclear. A monomer (MOCMTES) containing an ester unit with a low affinity for CO_2 was also examined, and its copolymerization with TEOS provided a membrane with high CO_2 permeance ($P_{CO2} = 2.074 \times 10^{-6}$ mol m^{-2}s^{-1} Pa^{-1}) and a moderate level of permselectivity ($CO_2/N_2 = 7.5$) [23]. Aromatic rings were also investigated as rigid CO_2-philic units. Their rigidity was expected to enhance intramolecular void formation, thus facilitating gas permeation. The membranes obtained by the copolymerization of phenyl-, pyridyl-, and naphthyl-containing triethoxysilane monomers (TESEB, TESEPy, and TESENp) with BTESE at a ratio of 1:1 exhibited good performance depending on the CO_2 affinity of the aromatic units, and the TESEB–BTESE and TESEPy–BTESE membranes exhibited good performance, with $P_{CO2} = 1.36 \times 10^{-7}$ mol m^{-2}s^{-1}Pa^{-1} and 3.34×10^{-7} mol m^{-2}s^{-1}Pa^{-1}, respectively, and $CO_2/N_2 = 16.5$ and 27.9, respectively [24]. However, the performance of the TESENp–BTESE membrane was inferior ($P_{CO2} = 2.05 \times 10^{-8}$ mol m^{-2}s^{-1}Pa^{-1} and $CO_2/N_2 = 14.4$), presumably because the formation of a π-stacked naphthalene dimeric form reduced the CO_2 affinity and densified the membrane. Pinacol borate was also introduced as a non-aromatic rigid unit with moderate CO_2 affinity to yield a membrane characterized by high CO_2 permeance ($P_{CO2} = 2.10 \times 10^{-6}$ mol m^{-2}s^{-1}Pa^{-1}) and relatively high permselectivity ($CO_2/N_2 = 11.1$) by 1:2 copolymerization with BTESE [25].

Bridged trialkoxysilanes have also been investigated as monomers, which may enhance the network structure of membranes. Among them, TTESMI and TTESPI, which contain a rigid CO_2-philic isocyanurate core, yielded good membranes with $P_{CO2} = 2.0 \times 10^{-7}$ and 3.2×10^{-7} mol m^{-2}s^{-1}Pa^{-1} and $CO_2/N_2 = 15$ and 18, respectively [26]. When TTESPI and BTESE were copolymerized at a 1:1 ratio, the resulting membrane exhibited improved CO_2 permeance, although its permselectivity was slightly reduced. These values are slightly higher than those of less rigid BTESPU membranes with urea units [26]. In addition to the appropriately high CO_2 affinity of organic units, their rigidity, which enhances void formation, is important for enhancing gas permeation. Additionally, the copolymerization of BTESB and BTESBPh with BTESA resulted in high-performance membranes for CO_2 separation. Interestingly, the copolymerization of BTESA with BTESB resulted in an increase in CO_2/N_2 permselectivity compared with that of the BTESA homopolymer membrane ($P_{CO2} = 1.84 \times 10^{-6}$ mol m^{-2}s^{-1}Pa^{-1}, $CO_2/N_2 = 25$), whereas the incorporation of BTESBPh increased the CO_2

permeance ($P_{CO2} = 3.25 \times 10^{-6}$ mol m^{-2}s^{-1}Pa^{-1}, $CO_2/N_2 = 12$) [28]. This is likely due to the higher CO_2 affinity of the benzene ring than that of the acetylene bond and the rigid biphenylene linkage, which expands the silica network to enhance gas permeation.

These results indicate that the CO_2 affinity of the membranes plays a significant role in their performance. However, other characteristics of organic units, such as rigidity, steric bulkiness, and the number of reactive silicon sites, operate synergistically together with CO_2 affinity to affect membrane separation performance, and predicting membrane performance by simple molecular design seems difficult. In addition, membrane preparation processes seem to affect performance. Considering the complexity of the performance prediction of PSQ membranes, we examined machine learning using the experimental data collected in our previous studies to create a prediction model for PSQ-based CO_2 separation membranes. The resulting model was used to predict the performance of new urea-containing membranes. The prepared membranes exhibited good to high performance. The influence of the calcination temperature on the preparation of PSQ membranes was also studied, and a new method for enhancing CO_2 permeability by controlling the thermal decomposition of urea units was proposed.

Materials and methods

Machine learning for the prediction of membrane performance

To predict the performance of PSQ-based membranes with different organic groups, Gaussian process regression was employed with the experimental data collected in our previous studies. The prepared dataset consisted of 132 entries of PSQ-based membranes prepared by homo- and copolymerization of alkoxysilane precursors, as presented in Fig. S1. The CO_2 permeance and CO_2/N_2 permselectivity were defined as the target variables, and the raw data used to obtain the explanatory variables are listed in Table S1: the amount of HCl catalyst (hereafter denoted as HCl), the temperature of the measurement (temp), the molecular weight of the monomer (MW), the CO_2 coordination energy for each monomer (H) evaluated at the B3LYP/6-31 G level of calculation on Gaussian 16 revision C.01 (Gaussian, Inc., USA), the number of acidic and basic moieties (an and bn, respectively), the degree of unsaturation in the organic groups (un), and the average distance between Si atoms (Si–Si) evaluated by Chem3D 23.1.2 (PerkinElmer Informatics Inc., USA). The corresponding variables for copolymers were evaluated as weighted averages for composing monomers on the basis of their weight ratio (Table S2). In addition, three binary descriptors, SiNoOne, SiNoTwo, and SiNoThree, were introduced, which have a value of one when the number of Si atoms in the monomer was one/two/three, respectively.

Materials and characterization

BTESE was obtained from Gelest, Inc., and was used as received. Monomers, (3,6-dioxaoctane-1,8-diyl)bis-*N*-[*N*'-(triethoxysillylpropyl)urea] (BTESEgU) and (triethylamine-2,2',2"-triyl)tris-*N*-[*N*'-(tri-ethoxysillylpropyl)urea] (TTESPUEA), were prepared as previously reported [29]. Ethanol used for the sol–gel reactions was distilled from magnesium ethoxide under an argon atmosphere and stored on activated molecular sieves in the dark until use. The sol particle sizes were measured by dynamic light scattering (DLS) using a Malvern Zetasizer Nano ZS analyzer at room temperature. Fourier transform infrared (FTIR) spectra were obtained using a Shimadzu IR Affinity-1 spectrometer. Thermogravimetric analysis (TGA) was performed using a Shimadzu DTG-60 thermal analyzer with a heating rate of 10 °C/min under a gentle nitrogen flow (100 mL/min).

Sol preparation

The sols were prepared according to a previously described method [26]. Water was added to stirred ethanol solutions of BTESEgU–BTESE and TTESPUEA–BTESE in a 1:1 weight ratio, and the mixtures were stirred further until the average sol particle sizes reached approximately 2 nm (Table 1). The resulting sols were diluted with ethanol to 0.25 wt% on the basis of the monomers used for the reactions. The sols were stored at 4 °C in tightly sealed screw vials until they were used. Drying the sols by heating at 60 °C in air provided the powders for TGA. For FTIR analysis, the sols were applied to a KBr plate and dried at 50 °C in air. The plates were subsequently heated at various temperatures for 10 min in nitrogen, and the spectra were collected in transmission mode.

Table 1 Conditions for sol formation-

Precursor /g (/mmol)	BTESE /g (/mmol)	Ethanol /g	Water /g	Reaction temperature/°C	Reaction time/h
BTESEgU 0.250 (0.39)	0.250 (0.71)	7.530	1.971	50	24
TTESPUEA 0.250 (0.28)	0.250 (0.71)	7.367	2.133	25	24

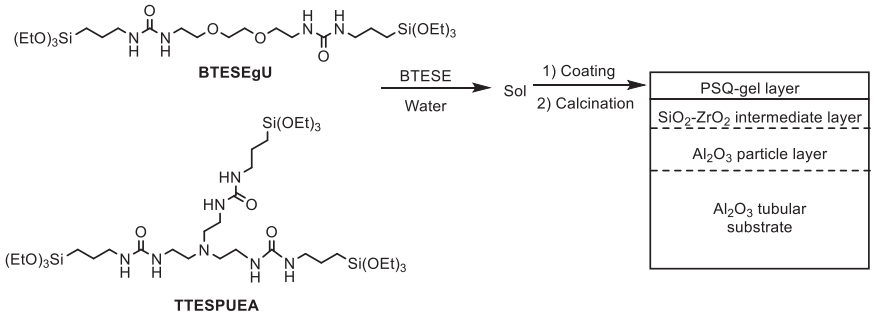

Fig. 2 Preparation of the CO_2 separation membrane

Membrane preparation

As described in a previous study [30], the support membrane was prepared using a commercially available porous tubular α-Al_2O_3 substrate (10 mm diameter, 1 μm average pore size). Initially, an aqueous colloidal α-Al_2O_3 sol was coated onto the tubular substrate, and the coated substrate was calcined. Subsequently, an intermediate layer with an approximate pore size of 1.5 nm was prepared by coating the substrate with silica-zirconia sols with different particle sizes, followed by calcination. Finally, a BTESEgU–BTESE or TTESPUEA–BTESE sol was coated onto the intermediate layer surface. The coated substrates were then calcined at 300 °C or 250 °C for 30 min in nitrogen for the preparation of a PSQ top layer (Fig. 2). The procedures of PSQ sol coating and subsequent calcination were conducted twice. Pure gases (He, H_2, CO_2, N_2, and SF_6) were fed into the membrane module at approximately 200 kPa. The gas permeance (P) was calculated using Eq. (1). The gas permeances that stabilized several hours after the gas permeation experiments were initiated are summarized in Table 2.

$$P = V/(22.4 \times A \times \Delta P) \quad (1)$$

ΔP: difference in pressure between the upstream and downstream sides of the membrane
V: flow rate of the permeated gas
A: effective membrane surface area

Results and discussion

Machine learning

There have been several reports on the construction of prediction models through machine learning for CO_2 separation in organic polymer membranes [32–35]. However, no studies have been conducted on PSQ-based membranes to date. In this study, a new model was created for PSQ-based membranes. The fivefold cross-validated values for CO_2 permeance and CO_2/N_2 permselectivity in the prepared dataset are plotted against the experimental values in Fig. 3. The corresponding R^2_{CV} (cross-validated R-squared) values indicating the generalization of model performance are 0.763 for CO_2 permeance and 0.507 for CO_2/N_2 permselectivity. CO_2 permeance was better modeled than CO_2/N_2 permselectivity was, while both models tended to underestimate the experimental values in high-performance regions.

Table 2 Predicted performance of the candidates by the Gaussian process model-

Precursor (weight ratio)	Measurement temperature/°C	P_{CO2} /mol $m^{-2}s^{-1}Pa^{-1}$	CO_2/N_2
HETESPU:BTESE (1:1)	50	1.3×10^{-7}	16
TTESPUEA:BTESE (1:1)	50	4.0×10^{-7}	8.0
BTESAU:BTESE (1:1)	50	2.4×10^{-7}	9.2
BTSUmX:BTESE (1:1)	50	2.6×10^{-7}	10
BTESEgU:BTESE (1:1)	50	2.7×10^{-7}	9.3

With this trained Gaussian process model, the performance of the five monomer candidates of the precursors (Fig. 2 and Fig. 4) was predicted, as shown in Table 2. These candidates were designed on the basis of our previous study that indicated the potential of urea-based PSQ membranes for CO_2 separation [26, 27]. The high rigidity and moderate CO_2 affinity of urea were anticipated to enhance CO_2 permeation. In addition, the structural rigidity and CO_2 affinity of amine [17–22], arene [24], and ethylene glycol units [36] were considered in the design of monomer candidates. Compared with those of the training dataset, the CO_2 permeance and CO_2/N_2 permselectivity of the candidates were found to have moderate performance with a trade-off relationship. Given the worse R^2_{CV} score for CO_2/N_2 permselectivity, TTESPUEA:BTESE and BTESEgU:BTESE were concluded to be the best choices among the five candidates.

When the experimental data obtained for the BTESEgU–BTESE and TTESPUEA–BTESE membranes (*vide infra*) were added, a revised model was obtained with an improved R^2_{CV} score for CO_2/N_2 permselectivity (0.596), although the score for CO_2 permeance was not

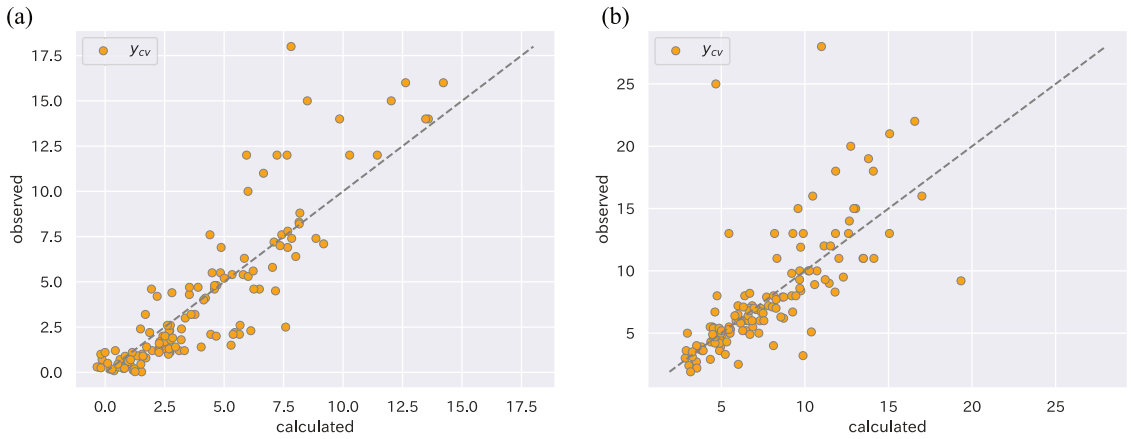

Fig. 3 Cross-validated values for (**a**) CO_2 permeance [10^{-7} mol $m^{-2}s^{-1}Pa^{-1}$] and **b** CO_2/N_2 permselectivity

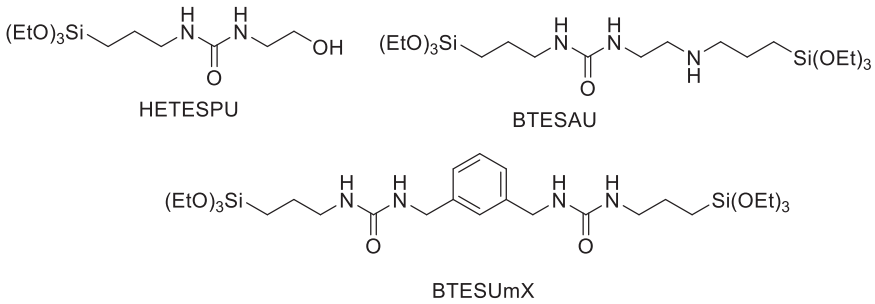

Fig. 4 Chemical structures of the monomer candidates: HETESPU, BTESAU, and BTESUmX

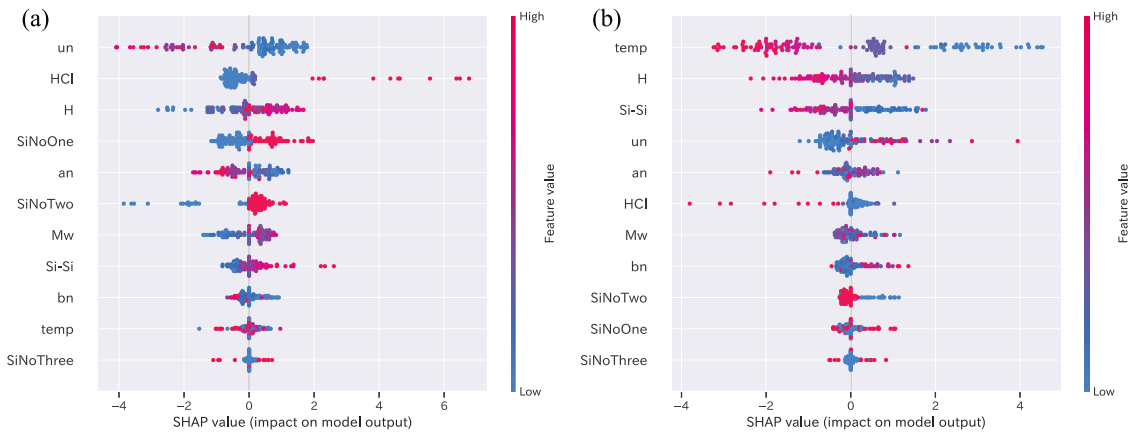

Fig. 5 Results of SHAP analysis for (**a**) CO_2 permeance and **b** CO_2/N_2 permselectivity. The top 3 significant features for CO_2 permeance based on the mean absolute SHAP values are the degree of unsaturation in the organic groups (un), the amount of HCl catalyst (HCl), and the CO_2 coordination energy (H), whereas those for CO_2/N_2 permselectivity are the operation temperature (temp), CO_2 coordination energy, and the average distance between Si atoms (Si–Si). The other features are described in the Materials and methods section

clearly affected (0.762). Shapley additive explanations (SHAP) were examined for the revised model, and the results are shown in Fig. 5. Interestingly, the CO_2 coordination energy (denoted as "H" in Fig. 5) strongly contributed to both the CO_2 permeance and CO_2/N_2 permeselectivity, which were positively correlated with the former and negatively correlated with CO_2/N_2 with the latter, indicating that the CO_2 coordination energy affected the performance as a trade-off factor for these parameters. Among the explanatory variables other than the CO_2 coordination energy, the degree of unsaturation of the organic unit (denoted as "un") and the amount of HCl catalyst for PSQ preparation (denoted as "HCl") strongly contributed to CO_2 permeance, whereas the measurement temperature, Si–Si distance (denoted as "Si–Si"), and degree of unsaturation influenced CO_2/N_2 permselectivity.

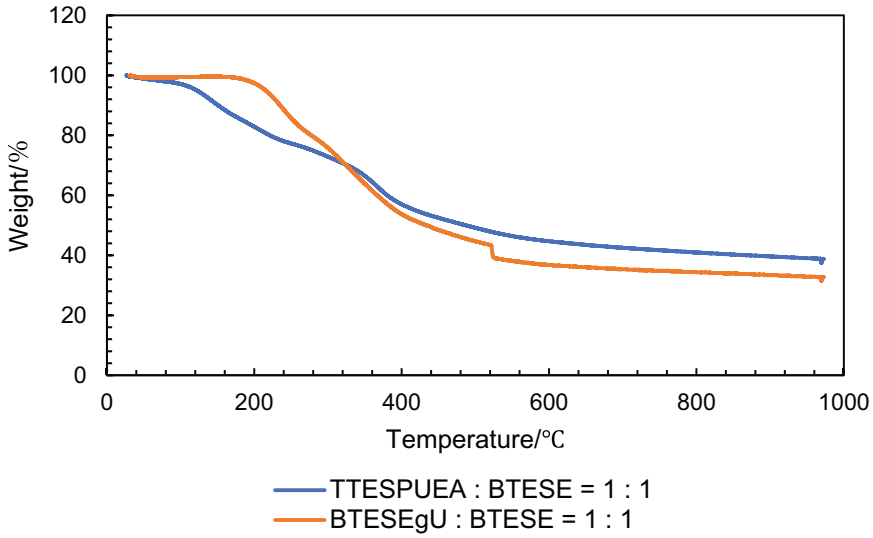

Fig. 6 TGA curves of BTESEgU–BTESE and TTESPUEA–BTESE gels in nitrogen

The increased degree of unsaturation reflected the enhanced rigidity of the organic unit, which accelerated CO_2 permeation. However, the introduction of π-electron systems increased the CO_2 affinity to improve the CO_2/N_2 permselectivity and to suppress the permeation. HCl catalysts have been used for the preparation of amine-containing PSQ to enhance polymerization. However, HCl remains in the membrane as an ammonium salt, which improves the CO_2 permeance with reduced CO_2/N_2 permselectivity [21]. The origin of the HCl effects remains unclear but is in accordance with the SHAP results. The most significant feature for CO_2/N_2 selectivity was the operation temperature, whose influence was negative at higher temperatures, suggesting that higher molecular mobility could obscure molecular differences. Similar temperature effects have been reported for polyethylene glycol-based membranes [34].

Membrane preparation

The urea-containing monomers were copolymerized with BTESE in a 1:1 weight ratio with excess water in ethanol. The reaction mixtures were stirred until the resulting sol particles increased in size slightly beyond the pore size (1.5 nm) of the intermediate layer of the support membrane so that the sol did not penetrate the intermediate layer. The reaction of BTESEgU proceeded less rapidly than that of TTESPUEA did, and its reaction should be carried out at a higher temperature to complete the reaction within a reasonable time. The lower reactivity of BTESEgU is presumably due to the smaller number of reactive triethoxysilyl units and the lack of an amine unit that would catalyze hydrolysis/condensation. The obtained sols were applied to the intermediate layer of the support membrane, and the coated sols were dried and subjected to calcination in nitrogen to form a gel separation layer. To determine the calcination temperature, TGA was performed on the BTESEgU–BTESE and TTESPUEA–BTESE gels prepared by drying the sols (Fig. 6). FTIR spectra of the gels were also obtained after heating at various temperatures for 10 min in nitrogen (Fig. 7).

The TGA curves indicated that the BTESEgU–BTESE and TTESPUEA–BTESE gels underwent a two-step weight loss: the first occurred up to 250–300 °C, and the second occurred at higher temperatures extending up to 500–600 °C. Their FTIR spectra revealed that the intensities of the stretching peaks of O–H and Si–OH bonds at approximately 3350 cm^{-1} and 950 cm^{-1}, respectively, weakened with increasing calcination temperature. An increase in the band at approximately 1000 cm^{-1}, ascribed to Si–O–Si stretching, was also observed, indicating that the dehydration condensation of silanols to form siloxanes occurred. For the TTESPUEA–BTESE gel, the Si–OH stretching band at approximately 950 cm^{-1} remained even after heating at 250 °C, in contrast to the BTESEgU–BTESE gel, whose FTIR spectrum showed the disappearance of the Si–OH band after heating at the same temperature. This is likely due to the greater steric hindrance of TTESPUEA than BTESEgU, which suppresses silanol condensation. Two intense signals characteristic of urea C = O and N–H bonds were observed for each sample at approximately 1600 cm^{-1} [37]. However, the urea signals weakened when the TTESPUEA–BTESE gel was heated to 300 °C, suggesting that thermal decomposition occurred at this temperature to some extent, whereas the spectrum of the BTESEgU–BTESE gel heated to 300 °C did not show significant changes in the urea signals. Notably, the Si–OH band at approximately 950 cm^{-1} almost disappeared in the TTESPUEA–BTESE spectra after heating at 300 °C, including silanol condensation. On the basis of these results,

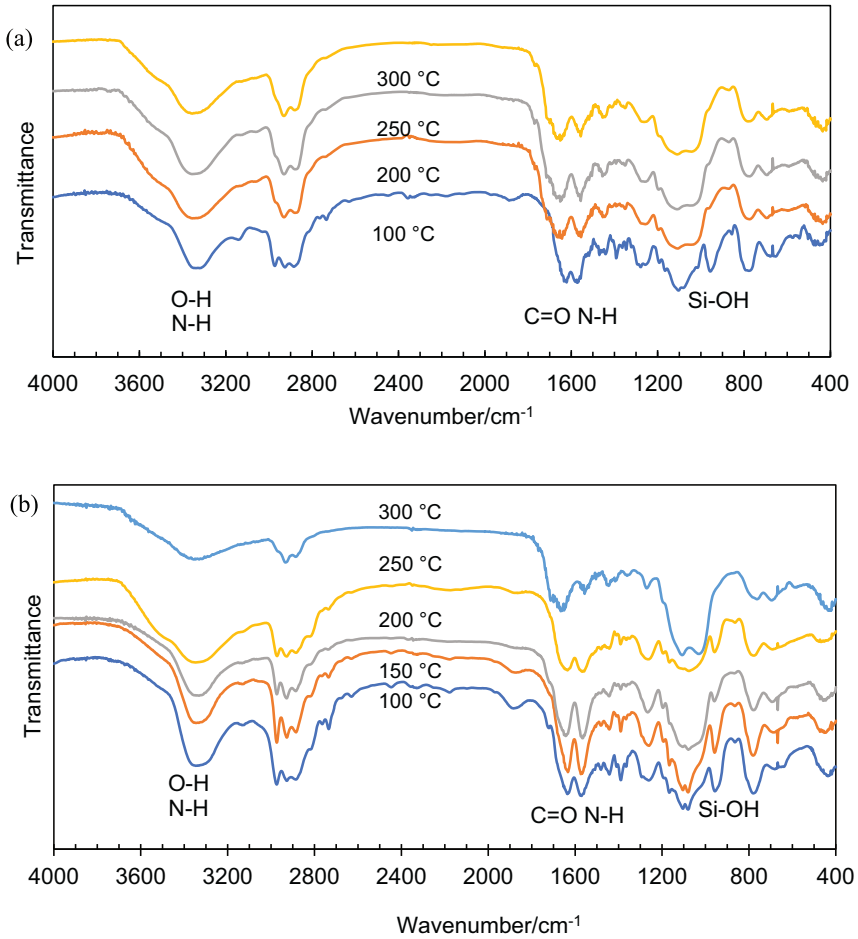

Fig. 7 IR spectra of (**a**) BTESEgU–BTESE and **b** TTESPUEA–BTESE gel films prepared on KBr plates after heating at different temperatures for 10 min in nitrogen

the membranes were prepared by calcination at 300 °C and 250 °C in nitrogen for the preparation of the BTESEgU–BTESE and TTESPUEA–BTESE separation membranes, respectively. TTESPUEA–BTESE was also calcined at 300 °C to elucidate how the thermal degradation of urea units affects membrane performance.

Evaluation of CO_2 separation properties

Pure gas permeation experiments were conducted at 200 °C for the BTESEgU–BTESE (300 °C) and TTESPUEA–BTESE (250 and 300 °C) membranes, where the values in parentheses denote the respective calcination temperatures. The resulting gas permeances are plotted against the gas kinetic diameter in Fig. 8a. The normalized permeation data and theoretical Knudsen diffusion line are presented in Fig. 8b. Relative to the Knudsen line, the observed permeances were more significantly suppressed when the gas kinetic diameter increased from H_2 to SF_6. This trend clearly suggests that gas transport through the membranes is influenced by molecular size, which is indicative of molecular sieving effects. Notably, the CO_2 permeances of the BTESEgU–BTESE (300 °C) and TTESPUEA–BTESE (300 °C) membranes exceeded the values predicted by the Knudsen model, implying a preferential interaction between the CO_2 molecules and the membrane structures. The CO_2 permeance and CO_2/N_2 permselectivity determined at 50 °C are listed in Table 3. The literature data for membranes synthesized via the homopolymerization of BTESE [25] and the 1:1 copolymerization of BTESPU and BTESE are also presented [26].

To further elucidate the gas transport mechanism, temperature-dependent gas permeation measurements were performed to determine the activation energies of CO_2 and N_2 permeation through the membranes (Fig. 9 and Table 3). Compared with N_2, all the present membranes demonstrated lower activation energies for the permeation of CO_2, which is consistent with an adsorption-controlled transport mechanism. Reduced operating temperatures increase CO_2 absorption by the membrane, thereby facilitating its permeation. Generally, lower activation energies are observed for inorganic membranes than for organic membranes because of the higher rigidity of inorganic structures, which are relatively unaffected by temperature. In contrast, the vibration of more flexible organic networks is readily enhanced at elevated temperatures compared with that of

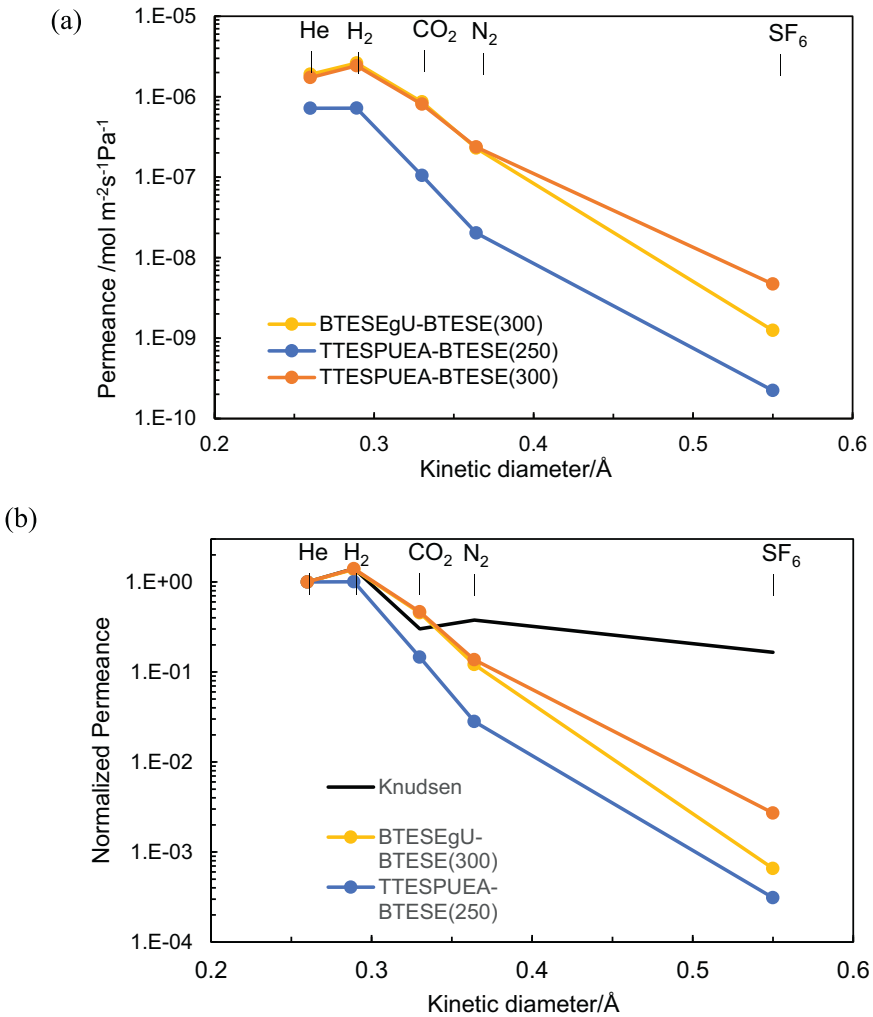

Fig. 8 **a** Plots of pure gas permeances of urea-containing PSQ membranes measured at 200 °C versus gas kinetic diameter. **b** Normalized data and Knudsen prediction based on helium gas permeance

Table 3 Gas permeation properties of the urea-containing membranes-

Precursor	Calcination temperature/°C	P_{CO2} /mol m^{-2}s^{-1}Pa^{-1} [a]	CO_2/N_2 [1]	E_{act}/kJmol^{-1} [b] CO_2	N_2
BTESEgU–BTESE (1:1)	300	1.3×10^{-6}	13	–3.8	5.2
TTESPUEA–BTESE (1:1)	250	5.1×10^{-8}	11	6.1	15
TTESPUEA–BTESE (1:1)	300	1.4×10^{-6}	8.1	-4.9	1.5
BTESPU–BTESE (1:1)[c]	300	2.2×10^{-7}	13	0.3	9.1
BTESE[d]	300	5.5×10^{-7}	13	-4.5	2.4

[a]Measured at 50 °C

[b]Activation energy for gas permeation

[c]Reference [26]

[d]Reference [25]

inorganic membranes to accelerate gas transport. The activation energy of N_2 permeation of the BTESEgU–BTESE (300 °C) membrane was nearly the same as that of the BTESPU–BTESE and BETSE membranes, indicating similar network rigidity. The higher activation energy of N_2 permeation for TTESPUEA–BTESE (250 °C) is likely due to the lower calcination temperature, leading to incomplete condensation, as indicated by the IR spectral analysis (*vide supra*). However, the value decreased for the TTESPUEA–BTESE (300 °C) membrane, indicating enhanced network formation by higher-temperature calcination. In terms of the CO_2 separation performance, the

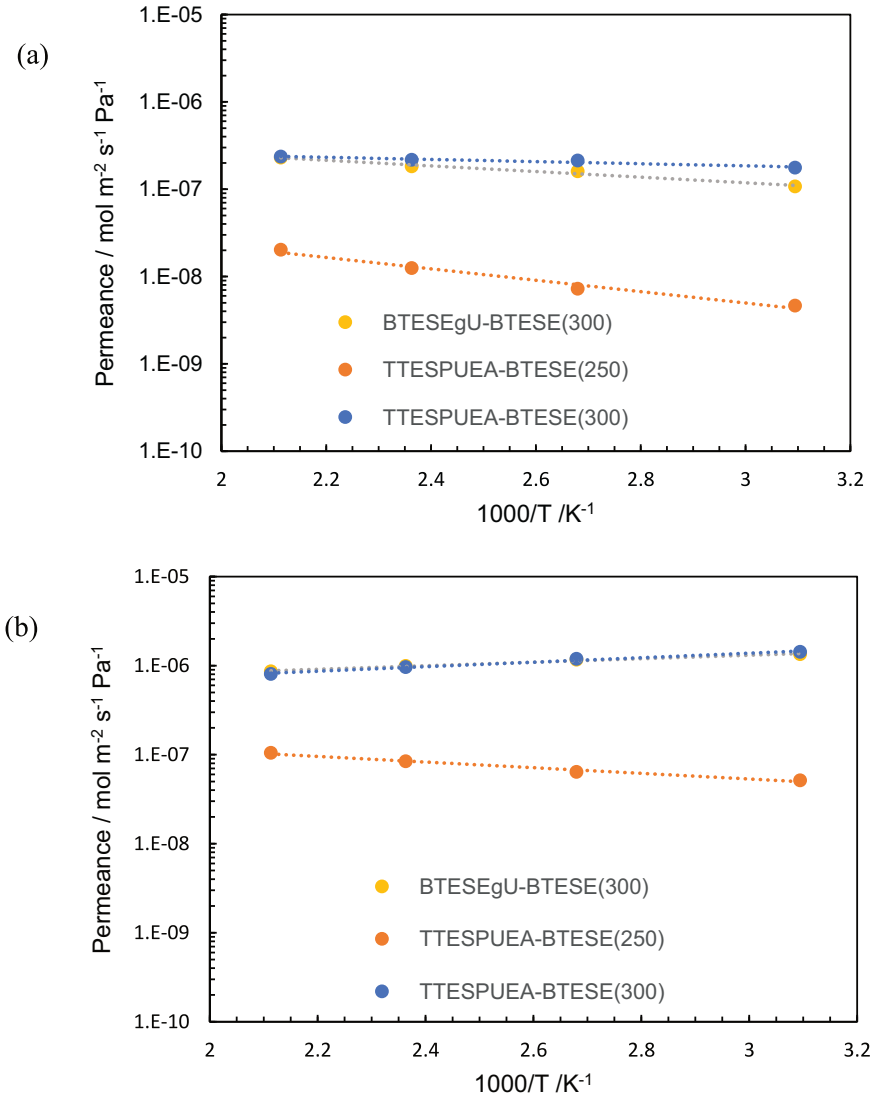

Fig. 9 Plots of gas permeances of (**a**) N_2 and **b** CO_2 versus operating temperatures for urea-containing membranes

BTESEgU–BTESE (300 °C) membrane exhibited the best data, with the highest CO_2 permeance ($P_{CO2} = 1.3 \times 10^{-6}$ mol m^{-2}s^{-1}Pa^{-1}) and moderately high CO_2/N_2 permselectivity ($CO_2/N_2 = 13$). This seems to be partly due to the enhanced siloxane network formation, as evidenced by the disappearance of the Si–OH bands in the IR spectrum after calcination at 300 °C (Fig. 7a). The presence of multiple CO_2-philic urea and ethylene glycol sites with appropriate CO_2 affinity could also explain the high performance of this membrane. Notably, the CO_2 permeance of the BTESEgU–BTESE (300 °C) membrane was much greater than that of the BTESPU–BTESE and BTESE membranes. In contrast, the TTESPUEA–BTESE (250 °C) membrane exhibited lower CO_2 permeance. As observed for the DMAPTES membrane, tertiary amine units have the potential to realize high CO_2 separation properties because of their appropriately high CO_2 affinity [17, 18]. However, the steric bulkiness of the tertiary amine unit in TTESPUEA

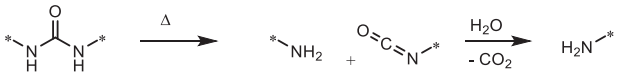

Fig. 10 Thermal degradation of *N*,*N*'-disubstituted urea followed by hydrolysis

overrides the effects of its CO_2 affinity, suppressing permeation (*vide infra*). Incomplete network formation is also a reason for the low CO_2 permeance. Interestingly, the permeation was markedly improved by calcination at 300 °C, and the P_{CO2} value of the TTESPUEA–BTESE (300 °C) membrane was 27 times greater than that of TTESPUEA–BTESE (250 °C), although the permselectivity decreased from $CO_2/N_2 = 11$ to 8.1. It has been reported that *N*,*N*'-disubstituted urea undergoes thermal degradation to form primary amine and isocyanate units [38]. The isocyanate group reacts with moisture to provide another primary amine unit and CO_2 (Fig. 10). As the membrane

contains hydrophilic urea units, it is not unexpected for the membrane to retain moisture even after calcination. Consequently, the membrane becomes looser, accelerating CO_2 permeation [39].

To compare the performance, the P_{CO2} and CO_2/N_2 values of the presently and previously prepared PSQ-based membranes are plotted in Fig. 11. As shown in Fig. 11, the CO_2 separation performance of the BTESEgU–BTESE (300 °C) membrane was superior to that of most PSQ-based membranes reported thus far, approaching the highest level of performance achieved by the BPinTES–BTESE, BTESB–BTESA, and BTESBPh–BTESA membranes.

CO_2 affinity

To evaluate the CO_2 affinity of the BTESEgU- and TTESPUEA-based membranes, the coordination energies of CO_2 with the BTESEgU and TTESPUEA (BSEgU and TSPUEA) models were calculated at the B3LYP/6-31 G level. The optimized geometries of the complexes and their coordination energies are shown in Fig. 12, indicating that they possess appropriately high CO_2 affinity. For BSEgU, a geometry with NH--O intramolecular hydrogen bonding was found to be the most stable among those examined, and CO_2 coordinates either the urea or the ethylene glycol unit. The coordination to urea was calculated to be more favorable than that to ethylene glycol, and the heat of the former reaction was used as an explanatory variable for prediction by the model. However, in a real system, the presence of multiple coordination sites affects CO_2 permeation, as mentioned above. Further studies may be necessary to understand these effects in detail.

For TSPUEA, two of the urea units were calculated to possess an intramolecular dimeric form by hydrogen bonding, making the coordination of CO_2 to this dimeric site difficult. Therefore, only the coordination to the unpaired urea site shown in Fig. 12c was considered, and the data were used as the explanatory variable. No stable CO_2 complexes coordinated to the tertiary amine unit of TSPUEA were obtained, likely because of steric repulsion between CO_2 and the substituents on the nitrogen atom.

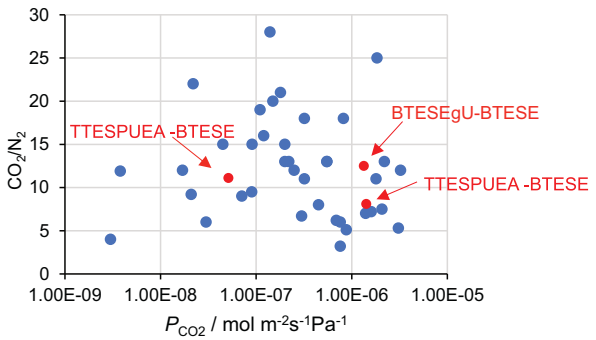

Fig. 11 Plots of P_{CO2} versus CO_2/N_2 for PSQ-based membranes. Red plots indicate the data of the membranes prepared in this study

Conclusions

In conclusion, two new urea-containing PSQ membranes were prepared, and their CO_2 separation performance was evaluated. Among them, the BTESEgU–BTESE (300 °C) membrane exhibited high performance, with $P_{CO2} = 1.3 \times 10^{-6}$ mol m^{-2}s^{-1}Pa^{-1} and a $CO_2/N_2 = 13$. In contrast, the TTESPUEA–BTESE (250 °C) membrane exhibited a significantly lower P_{CO2} value. A prediction model for CO_2 permeance and CO_2/N_2 permselectivity as target variables was generated using machine learning based on experimental data collected in our previous studies as explanatory variables. The model has potential application for the design of the chemical structure of membranes, although the accuracy of the prediction model is not very high. The accuracy is improved by the addition of more experimental explanatory variables. Notably, the calcination of TTESPUEA–BTESE at higher temperatures resulted in a drastic improvement in membrane performance. This seems to be an effective methodology for optimizing the chemical structure of membranes. The CO_2 separation performance of the BTESEgU–BTESE (300 °C) membranes ranks in the top tier of PSQ-based membranes. Given the high stability and facile film-forming properties of PSQ materials, these results merit significant attention. Optimizing the membrane preparation process, monomer ratio, and comonomer structure is in progress.

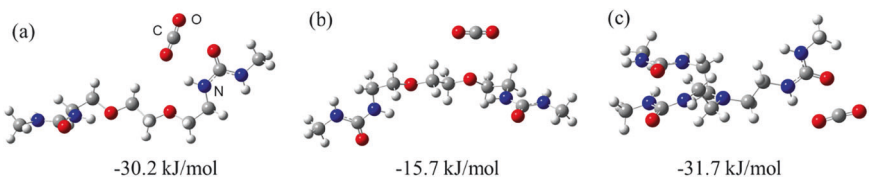

Fig. 12 Optimized geometries of CO_2 complexes of model compounds: **a** BSEgU coordinated at the urea site, **b** ethylene glycol unit site, and **c** TSPUEA, in which (triethoxysilyl)propyl groups of BTESEgU and TTESPUEA are replaced by methyl groups. The reaction heats for complex formation from the models and CO_2 molecules are also shown

Supplementary information

Supplementary information is available at the Polymer Journal website, which includes structures of precursors (Fig. S1), lists of raw data, and explanatory and target variables (Tables S1 and S2) for machine learning.

Funding Open Access funding provided by Hiroshima University.

Compliance with ethical standards

Conflict of interest The authors declare no competing interests.

Publisher's note Springer Nature remains neutral with regard to jurisdictional claims in published maps and institutional affiliations.

References

1. Robeson LM. The upper bound revisited. J Memb Sci. 2008;320:390–400.
2. Brunetti A, Scura F, Barbieri G, Drioli E. Membrane technologies for CO_2 separation. J Memb Sci. 2010;359:115–25.
3. Ma C, Wang M, Wang Z, Gao M, Wang J. Recent progress on thin film composite membranes for CO_2 separation. J CO2 Util. 2020;42:101296.
4. Dai Y, Niu Z, Luo W, Wang Y, Mu P, Li J. A review on the recent advances in composite membranes for CO_2 capture processes. Sep Purif Technol. 2023;307:122752.
5. Kamio E, Yoshioka T, Matsuyama H. Recent advances in carbon dioxide separation membranes: A review. J Chem Eng Jpn. 2023;56:2222000.
6. Tien-Binh N, Rodrigue D. Kliaguine S. In-situ cross interface linking of PIM-1 polymer and UiO-66-NH_2 for outstanding gas separation and physical aging control. J Memb Sci. 2018;548:429–38.
7. Duan K, Wang J, Zhang Y, Liu J. Covalent organic frameworks (COFs) functionalized mixed matrix membrane for effective CO_2/N_2 separation. J Memb Sci. 2019;572:588–95.
8. Zito PF, Caravella A, Brunetti A, Drioli E, Barbieri G. Knudsen and surface diffusion competing for gas permeation inside silicalite membranes. J Memb Sci. 2017;523:456–69.
9. Wang H, Wang M, Liang X, Yuan J, Yang H, Wang S, et al. Organic molecular sieve membranes for chemical separations. Chem Soc Rev. 2021;50:5468–516.
10. Fan Y, Yu W, Wu A, Shu W, Zhang Y. Recent progress on CO_2 separation membranes. RSC Adv. 2024;14:20714–34.
11. Abe Y, Gunji T. Oligo- and polysiloxanes. Prog Polym Sci. 2004;29:149–82.
12. Gon M, Tanaka K, Chujo Y. Recent progress in the development of advanced element-block materials. Polym J. 2018;50:109–26.
13. Du Y, Liu H. Cage-like silsesquioxanes-based hybrid materials. Dalton Trans. 2020;49:5396–405.
14. Kim J, Park Y, Kwon MS. Recent progress in ladder-like polysilsesquioxane: synthesis and applications. Mater Chem Front. 2024;8:2689–726.
15. Woo RK, Lee AS, Park SH, Baek KY, Lee KB, Lee SH, et al. Free-standing, polysilsesquioxane-based inorganic/organic hybrid membranes for gas separations. J Memb Sci. 2015;475:384–94.
16. Park S, Lee AS, Do YS, Hwang SS, Lee YM, Lee JH, et al. Rational molecular design of PEOlated ladder-structured polysilsesquioxane membranes for high performance CO_2 removal. Chem Commun. 2015;51:15308–11.
17. Yu L, Kanezashi M, Nagasawa H, Tsuru T. Role of amine type in CO_2 separation performance within amine functionalized silica/organosilica membranes: A review. Appl Sci. 2018;8:1032.
18. Yu L, Kanezashi M, Nagasawa H, Tsuru T. Fabrication and CO_2 permeation properties of amine-silica membranes using a variety of amine types. J Memb Sci. 2017;541:447–56.
19. Paradis GG, Kreiter R, van Tuel MM, Nijmeijer A, Vente JF. Amino-functionalized microporous hybrid silica membranes. J Mater Chem. 2012;22:7258–64.
20. Xomeriakis G, Tsai CY, Brnker CJ. Microporous sol–gel derived aminosilicate membrane for enhanced carbon dioxide separation. Sep Purif Technol. 2005;42:249–57.
21. Ohshita J, Okonogi T, Kajimura K, Horata K, Adachi Y, Kanezashi M, et al. Preparation of amine- and ammonium-containing polysilsesquioxane membranes for CO_2 separation. Polym J. 2022;54:875–82.
22. Karimi S, Mortazavi Y, Khodadadi AA, Holmgren A, Korelskiy D, Hedlund J. Functionalization of silica membranes for CO_2 separation. Sep Purif Technol. 2020;235:116207.
23. Karimi S, Korelskiy D, Mortazavi Y, Khodadadi AA, Sardar K, Esmaeili M, et al. High flux acetate functionalized silica membranes based on in-situ co-condensation for CO_2/N_2 separation. J Memb Sci. 2016;520:574–82.
24. Yoshio T, Horata K, Adachi Y, Tsuru T, Kanezashi M, Ohshita J. Effects of aryl substituents on the performance of polysilsesquioxane-based CO_2 separation membranes. J Sol -Gel Sci Technol. 2025;116:849–58.
25. Adachi Y, Yoshio T, Kajimura K, Sasaki K, Hara K, Kanezashi M, et al. Pinacol boronate ester-containing polysilsesquioxane membranes for CO_2 separation. ACS Appl Polym Mater. 2024;6:9744–51.
26. Kajimura K, Horata K, Adachi Y, Kanezashi M, Tsuru T, Ohshita J. Preparation of urea- and isocyanurate-containing polysilsesquioxane membranes for CO_2 separation. J Sol -Gel Sci Technol. 2023;106:149–57.
27. Mizumo T, Muragishi H, Yamamoto K, Ohshita J, Kanezashi M, Tsuru T. Preparation and separation properties of oxalylurea-bridged silica membranes. Appl Organomet Chem. 2015;29:433–8.
28. Guo M, Zhang Y, Xu R, Ren X, Huang W, Zhong J, et al. Ultrahigh permeation of CO_2 capture using composite organosilica membranes. Sep Purif Technol. 2022;282:120061.
29. Ohshita J, Horata K, Kaneko T, Adachi Y, Kanezashi M. Preparation of polysilsesquioxane-based RO membranes with urea units for water desalination. Membranes. 2025;15:322.
30. Tsuru T, Nakasuji T, Oka M, Kanezashi M, Yoshioka T. Preparation of hydrophobic nanoporous methylated SiO_2 membranes and application to nanofiltration of hexane solutions. J Memb Sci. 2011;384:149–56.
31. Ben Said R, Kolle JM, Essalah K, Tangour B, Sayari B. A unified approach to CO_2–amine reaction mechanisms. ACS Omega. 2020;5:26595–606.

32. Barnett JW, Connor B, Wang Y, Benicewicz B, Murdock LA, Bereau T, et al. Designing exceptional gas-separation polymer membranes using machine learning. Sci Adv. 2020;6:eaaz4301.
33. Zheng G, Zhang S, Meng L, Zhang S, Wang X. Machine learning-guided design and synthesis of eco-friendly polyethylene oxide membranes for high-efficacy CO_2/N_2 separation. Adv Funct Mater. 2024;34:2410075.
34. Basdogan Y, Pollard DR, Shastry T, Carbone MR, Kumar SK, Wang ZG. Machine learning-guided discovery of polymer membranes for CO_2 separation with genetic algorithm. J Membr Sci. 2024;712:123169.
35. Abdollahi F, Khosravi A, Karagöz S, Keshavarz A. A systematic review of recent advances in the application of machine learning in membrane-based gas separation technologies. Appl Energy. 2025;125203.
36. Park S, Lee AS, Do YS, Hwang SS, Lee YM, Lee JH, et al. Rational molecular design of PEOlated ladder-structured polysilsesquioxane membranes for high performance CO_2 removal. Chem Commun. 2015;51:15308.
37. Kamitani T, Ishida A, Imoto H, Naka K. Supramolecular organogel of polyureas containing POSS units in the main chain: dependence on POSS and co-monomer structures. Polym J. 2022;54:161–7.
38. Honorien J, Fournet R, Glaude PA, Sirjean B. Theoretical study of the thermal decomposition of urea derivatives. J Phys Chem A. 2022;126:6264–77.
39. Horata K, Yoshio T, Miyazaki R, Adachi Y, Kanezashi M, Tsuru T, et al. Preparation of polysilsesquioxane-based CO_2 separation membranes with thermally degradable succinic anhydride and urea units. Separations. 2024;11:110.